PHASE SATURATION VALIDATION AND TRACER TRANSPORT QUANTIFICATION USING MICROPET IN A HETEROGENEOUS SANDSTONE CORE

Christopher Zahasky and Sally M. Benson

Stanford University, Department of Energy Resources Engineering, 367 Panama St, Green Earth Sciences Building, Stanford, CA, 94305, USA

This paper was prepared for presentation at the International Symposium of the Society of Core Analysts held in Snow Mass, Colorado, USA, 21-26 August 2016

ABSTRACT

Quantification and measurement of core scale heterogeneity is of special interest because it is known to have a significant impact on multiphase displacement in porous media. Laboratory characterization of fluid flow behavior through heterogeneous sandstone cores is key for understanding and informing simulation models on realistic capillary trapping and continuum-scale relative permeability curves. To date, most of the studies pursuing this line of inquiry have relied on X-Ray Computed Tomography (CT) for measuring the sub-core scale rock properties. Here we describe the development of a relatively new experimental platform for these investigations, namely, micro Positron Emission Tomography (microPET). Positron Emission Tomography is a non-destructive, four dimensional, reproducible imaging technique that enables direct visualization of dynamic single phase and multiphase fluid flow in porous media at the continuum scale. The microPET scanner employed in this study is different from traditional PET scanners in that it is designed for pre-clinical, small animal imaging and thus has a much smaller system diameter than traditional clinical PET scanners. This smaller system size improves the fundamental resolution of PET imaging by about a factor of three [1]. While PET imaging has been utilized in a handful of studies for single and multiphase flow analysis in cores, we believe that with additional development, microPET could provide an important complement to CT based imaging techniques.

Through repeated experiments using microPET and CT to quantify phase saturations we are able to, for the first time, validate phase saturation measurements with microPET. We then use this data to develop sub-core scale permeability maps with the techniques developed in Krause et al, [2] and Pini et al, [3]. Using the sub-core scale permeability and porosity maps it is possible to approximate the transport properties of the core as a bundle of steamtubes. Finally, we compare microPET data from a single phase pulse tracer experiment to analytical solutions of the Advection-Dispersion Equation (ADE) for the entire core and the core described as a bundle of streamtubes.

INTRODUCTION

Recent advances in laboratory and theoretical techniques have led to the development of methods for quantifying capillary heterogeneity during core flooding experiments with X-ray CT [3,4] and using voxel based capillary pressure scaling to quantify the permeability field of entire core samples [2]. While Computed Tomography is the most widely used imaging technique for observing experimental multiphase flow behavior, it has a few important limitations. First, the temporal resolution for imaging dynamic flow behavior can be severely limited depending on the scanning and cool down speed of the particular scanner. PET provides continuous 3D images of the entire core throughout the duration of the experiment. During image reconstruction it is possible to discretize the PET scan into time steps as small as a few seconds—depending on radioactivity levels in the scanner. Second, when imaging single phase flow or flow of two fluids with similar attenuation coefficients it is necessary to add dopants to one or both of the fluids which may alter the density and/or chemical behavior of the fluids. Emission tomography techniques such as PET rely on very small concentrations of positron-emitting tracer. These low concentrations do not alter the density or chemical reactivity of the injected fluids. The flexibility of the dynamic image construction combined with the higher signal to noise ratio enables PET imaging to compliment CT imaging for studying various multiphase flow processes.

During a PET scan, positrons are emitted as consequence of a β^+ decay from the injected radiotracer. As they travel through the surrounding material they lose energy and slow down due mostly to electromagnetic collisions with surrounding atoms and molecules. As the velocity of the positron decreases there is an increasing probability that it combines with an electron and annihilates. This annihilation event produces two gamma rays emitted in nearly opposite directions, each with an energy of 511 keV. These pairs of coincident gamma rays are then detected with an array of photon detectors that surround the material containing the radiotracer (Figure 1). An event is registered by the system only if two coincident gamma rays strike two separate photon detectors within the coincidence window (4.5 ns).

Positron Emission Tomography relies on the artificial production of positron emitting radionuclides. Radionuclides are typically chosen based on desired half-life, radioactive decay emissions, radionuclide facility generation capabilities, and the chemical properties of tracer fluid. The radiotracer used in this study is Fludeoxyglucose (FDG) which incorporates the ^{18}F positron emitting isotope. The radiotracer is provided by the Stanford Radiochemistry Facility. This radioisotope was chosen because its half-life of 110 minutes is favorable for multi-hour scans. Simple pulse tests indicate there is little or no chemical interaction between the radiotracer and the porous media however chemical-rock analysis is ongoing.

PET imaging techniques have only been utilized in a handful of reservoir engineering and hydrology applications. Recently Pini et al, [5] used PET imaging of a ^{11}C radiotracer to quantify single phase advection and dispersion in a relatively heterogeneous Berea core.

Loggia et al, [6] used positron emission projection imaging (PEPI) to image flow through a fracture in a large limestone block (36 cm x 26 cm x 60 cm). They used a ^{64}Cu tracer to analyze geometrical dispersion, calculate fracture aperture, and quantify fluid channeling throughout the fracture. Spatial correlation analysis of the resulting fracture aperture was calculated. Kulenkampff et al, [7] used two different radiotracers [^{18}F]KF and [^{124}I]KI to image a large (roughly 0.5 mm aperture) axial fracture in a granite core. A peak-finding function was developed to identify the fracture location from the PET data, the results were compared with aperture measurements from a high resolution, micro CT scan of the same fracture. The only examples of high pressure experiments done with PET imaging were performed by Ferno et al, [8] and Maucec et al, [9]. In Maucec et al, [9], F18 was diluted in water and used to visualize flow through small (1 inch diameter) sandstone and fractured shale cores. Ferno et al, [8] performed single and multiphase experiments at reservoir conditions. This was the first study to describe a method for using PET images for calculating phase saturations, however these measurements were not validated with other saturation quantification techniques.

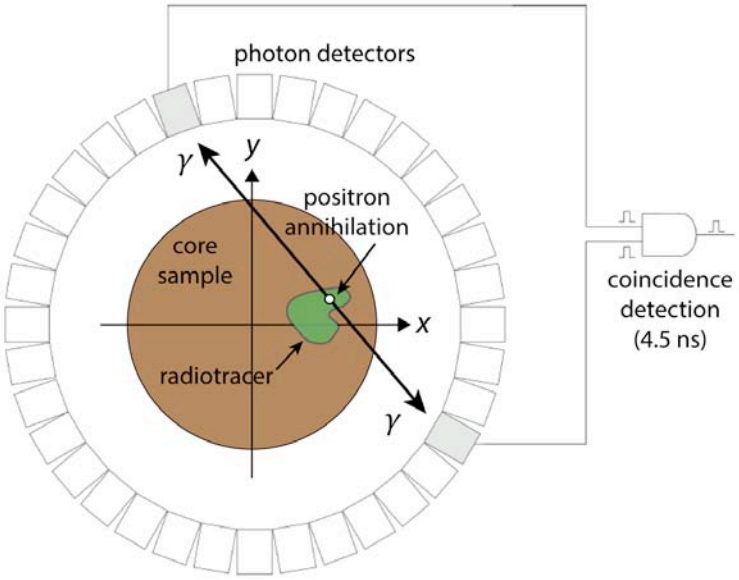

Figure 1: Schematic of positron annihilation event which creates two gamma rays that theoretically travel exactly 180^{o} from each other, striking the photon detectors in PET scanner within 4.5 nanoseconds of each other.

In this study, a water-nitrogen drainage experiment is performed in a 3.5 inch diameter Berea sandstone core first using CT to measure porosity and phase saturations and then using a preclinical microPET scanner to measure phase saturations in a second experiment. The microPET experiment had two stages. The first was a tracer pulse test in which a volume of tracer approximately equal to 10% of the core pore volume was injected and then displaced by water at the same flow rate. The second stage of the experiment was a tracer saturation and drainage experiment in which approximately 2 PV of radiotracer was injected into the core in order to fully saturate the wetting fluid (water) with tracer. Once the core was fully saturated with tracer, a simple drainage experiment

was performed in which nitrogen gas was injected at 10 mL/min and then 25 mL/min. The reduction in radiotracer in the core scales with the reduction in wetting phase saturation enabling phase saturation throughout the core. While the final PET saturation maps have a lower spatial resolution than the CT saturation maps, the saturation values between the experiments are in good agreement and thus provide validation that PET imaging can be used to provide quantitative saturation information.

Using methods such as those developed by Krause et al [4] it is possible to use the resulting core saturation maps in combination with MICP data to construct unique permeability maps describing the permeability in every voxel in the core. The in-situ tracer migration data collected from the PET scan is then used to validate these permeability maps by comparing the PET data with results from analytical ADE tracer transport calculations relying on the permeability maps to characterize the core scale model. Future work will further validate the PET transport through the use of numerical simulation.

METHODS

Experimental Setup

A schematic of the experimental setup used for these experiments is shown in Figure 2. The setup enables both single and multiphase fluid injection, radiotracer removal and shielding, and continuous collection of inlet and outlet pressure and radiotracer concentration data. Continuous water injection is achieved with a pair of Teledyne ISCO Model 500D syringe pumps and core outlet backpressure (typically around 100 psi) is maintained with an ISCO Model 1000D syringe pump. Gas is injected using a Sierra C100L gas mass flow controller rated to 500 psi. Confining pressure is applied with an ISCO 500D pump and is set to 400-450 psi for all experiments. Tracer is injected into the core from an additional ISCO 500D pump and is loaded using an NE-1000 programmable single syringe pump. Injected fluid passes through an inlet radioactivity detector prior to entering the sample holder. The effluent fluid then passes through an outlet radioactivity detector prior to being discharged into a waste container. Both differential (Omegadyne 150-DIFF-W/W-USBH) and absolute (Omegadyne 100-USBH) fluid pressure are measured at the inlet and outlet of the sample holder. Lead bricks and machined lead shielding is placed around several of the experiment components including the radioactivity detectors, injection syringe, tracer injection pump, backpressure pump, and the radioactivity waste reservoir. Shielding is used to reduce the radiation dose received by the experimenter and to reduce the background radiation that can increase noise during the microPET scans. The coreholder used in this study was custom built to fit in the microPET scanner and utilized a low attenuation cast nylon material for the outer confining shell. The inlet and outlet caps where machined from aluminum. There are two confining pressure ports on the inlet of the coreholder to enable temperature control via continuous fluid circulation between the coreholder and the confining pressure pump which contained a temperature control sleeve. The confining pressure water was circulated with an Eldex ReciPro Series 2000 reciprocating piston pump.

The PET scans are performed using a Siemens pre-clinical Inveon DPET scanner at the Stanford Center for Innovation in In-Vivo Imaging (SCI[3]). Prior to starting experiments, the core sample is loaded in the coreholder and scanned on a separate Siemens pre-clinical Inveon CT scanner. This CT scan is used to generate the attenuation correction map which is used for the scatter correction during the PET reconstruction.

A separate experiment was performed using only a GE Lightspeed clinical CT scanner in the Stanford Department of Energy Resources Engineering to acquire porosity and phase saturation maps in order to validate saturation measurements made during the PET experiment. The same experimental setup was used for the CT and PET experiments.

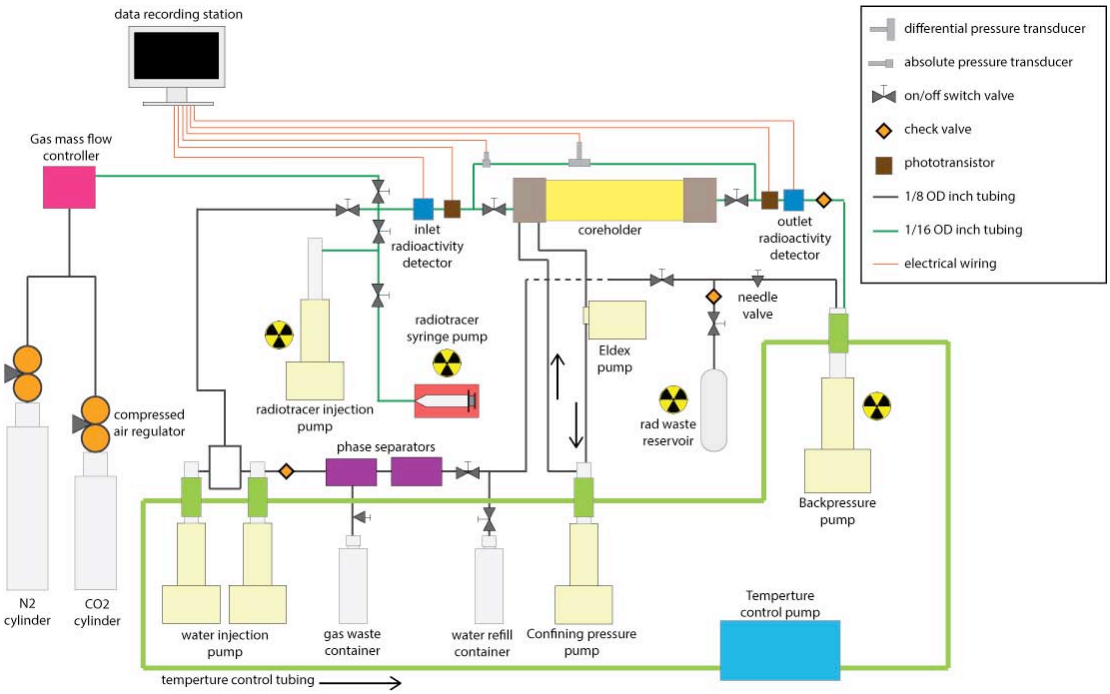

Figure 2: Schematic of experimental setup of single and multiphase PET experiments

CT Experimental Summary

The 3.5 inch diameter by 5.5 inch long Berea core was first dried in a vacuum oven for several days before being loaded into the coreholder. Following the dry CT scans, the core was saturated with gaseous CO_2 to displace all the air in the core. Next, tap water was injected continuously through the sample for over 24 hours at a flow rates of 10-20 mL/min and pressures between ambient and 150 psi. Water was removed from the system and replenished with fresh tap water three times in order be sure that all of the CO_2 originally in the core was either displace or dissolved into the water. Once the core was fully saturated with water five repeated wet CT scans were taken of the core.

Gas injection started at 5 mL/min and was injected continuously for over 12 hours (approximately 20 PV), with water injection completely shutoff. Five repeated CT scans were again taken. This process was repeated at gas flow rates 10, 15, 20, 25, and 30 mL/min except at each flow rate the volume of nitrogen injected was only 5-8 PV. Before increasing the gas flow rate five repeated CT scans were taken of the entire core.

PET Experimental Summary

Following the completion of the CT experiment, CO_2 was again injected at very high flow rates (~100 mL/min) and at pressures up to 100 psi in order to displace the nitrogen in the core. Water was then injected for approximately 48 hours at 10-20 mL/min. Water was removed from the system and fresh tap water was added to the system three times in order be sure the all the CO_2 in the core was either displaced or dissolved into the water.

Once the core was re-saturated with water, a short tracer injection followed by a drainage experiment were performed during a four hour microPET scan. Prior to starting the microPET scan, 4.2 millicurie of FDG was injected into the ISCO tracer pump containing 500 mL of water. In order to ensure proper mixing of the tracer and resident water the FDG solution was first diluted with approximately 50 mL of cold water. This diluted FDG solution was then injected into the warmer water in the ISCO pump and repeatedly injected and produced from the ISCO pump (set to constant pressure mode a 10 psi) six times. Once the FDG was well mixed in the ISCO pump, the microPET scan was started and the freshwater pump was shut off and tracer was injected for 150 seconds at 10 mL/min. After 25 mL of tracer was injected, the tracer pump was shutoff and freshwater injection immediately resumed at 10 mL/min. Approximately 2.5 PV of freshwater was injected, and the tracer pulse was completely displaced through the core as determined by the outlet radioactivity detector (first pulse of red curve in Figure 3). Following this stage of the experiment, 475 mL of radiotracer was injected continuously into the core until the core was fully saturated, again verified by inlet and outlet activity curves (Figure 3). Radiotracer injection is then shutoff and 6 PV of nitrogen is injected at 10 mL/min. During the last stage of the experiment the nitrogen flow rate is increased to 25 mL/min and approximately 6 PV of nitrogen is injected.

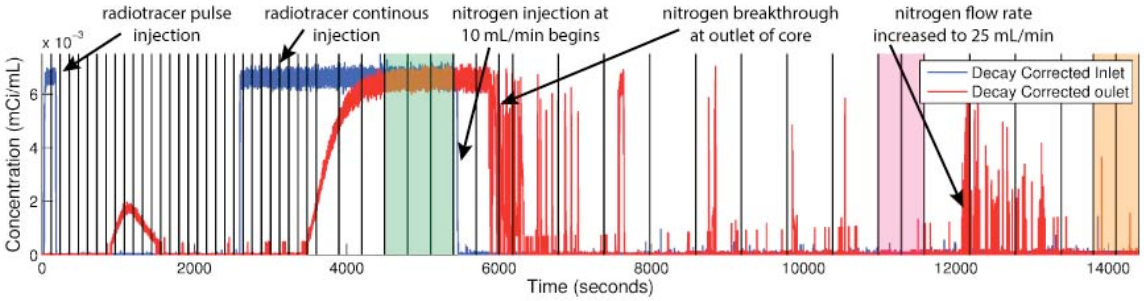

Figure 3: Decay corrected inlet and outlet tracer curves of multistage PET experiment. Vertical black lines indicate dynamic frame locations of PET scan reconstruction for phase saturation analysis.

Following the completion of the microPET scan, the continuously recorded coincident events are binned into desired timesteps (black vertical lines in Figure 3). These bins of coincident events are then used to reconstruct dynamic 3D images of the entire microPET scan. As a result of this process, each frame of the reconstructed images shows the average tracer location between the beginning and end time of that frame. One of the major benefits of PET imaging is that scans can be repeatedly reconstructed with different timestep specifications so that different stages of the experiment can be analyzed in detail long after the experiment is complete. The reconstruction method used for this study is the 3D Ordered Subset Expectation Maximization using Maximum A Priori (OSEM-OP MAP), an iterative reconstruction method [10]. The nominal resolution of the reconstructed images is 0.77 mm x 0.77 mm x 0.79 mm, however the images are coarsened up to 3.8 mm x 3.8 mm x 3.8 mm. Coarsening was performed to reduce noise in the microPET data. In part, this is due to a poor attenuation correction map used in the microPET reconstruction. Since this is the first study of its kind on this microPET scanner, we are in the process of developing new beam hardening and attenuation map calibration methods in order to improve the attenuation correction and spatial resolution of the measurements. For the sake of comparison, the CT scans were coarsened to similar voxel size. Coarsening was done by taking the arithmetic mean of the smaller voxels located in the resulting coarse voxels.

RESULTS

PET – CT Saturation Comparison

Once the microPET image is reconstructed, water saturation (S_w) is calculated as the linear interpolation of time-average activity concentration at steady state gas injection ($PET_{drainage}$) over the time-average activity concentration of the same voxel at full water/tracer saturation (PET_{ft}) as shown in Equation 1.

$$S_w = \frac{\mathrm{PET}_{drainage} - \mathrm{PET}_{pt}}{\mathrm{PET}_{ft} - \mathrm{PET}_{pt}} \qquad (1)$$

If the initial voxel tracer concentration (PET_{pt}) is zero then this simplifies to the saturation equation described in [8]. In order to calculate the time-averaged activity concentration at full water saturation the three frames in which tracer is flow in the inlet is equal to the tracer flow at the outlet are averaged (three frames highlighted in green in Figure 3). This frame averaging is done to improve the voxel statistics, similar to improvements gained by averaging repeated CT scans. The frames used to calculate the time average concentration of the steady state nitrogen injection at 10 mL/min are highlighted in pink and at 25 mL/min are highlighted in orange in Figure 3.

In order to calculate nitrogen saturations for each voxel from the CT experiment we rely on the linear interpolation between pure states as described by Equation 2 [11].

$$S_w = \frac{\mathrm{CT}_{drainage} - \mathrm{CT}_{gas}}{\mathrm{CT}_{water} - \mathrm{CT}_{gas}} \qquad (2)$$

Where $CT_{drainage}$ is determined from the average of the five scans taken at a specified nitrogen flow rate, CT_{gas} is calculated from the average of the five scans taken prior to

saturating the core with water, and CT_{water} is taken from the average of the five scans taken when the core is fully saturated with water.

A comparison of the slice average saturations from the microPET and CT drainage experiments is shown in Figure 4. The saturations at the inlet slice of the core and slices toward the center agree very well. There is some discrepancy between the saturation around 10 mm from the inlet of the core. We believe this is not due to errors in either the CT or microPET scans but the fact that initially the CT drainage experiment started by flowing roughly 20 PV of nitrogen through the core at 5 mL/min (flowing gas overnight) before increasing the flow rate to 10 mL/min whereas the PET scan experiment flowed only 6 PV of nitrogen through the core at 10 mL/min before increasing the flow rate to 25 mL/min.

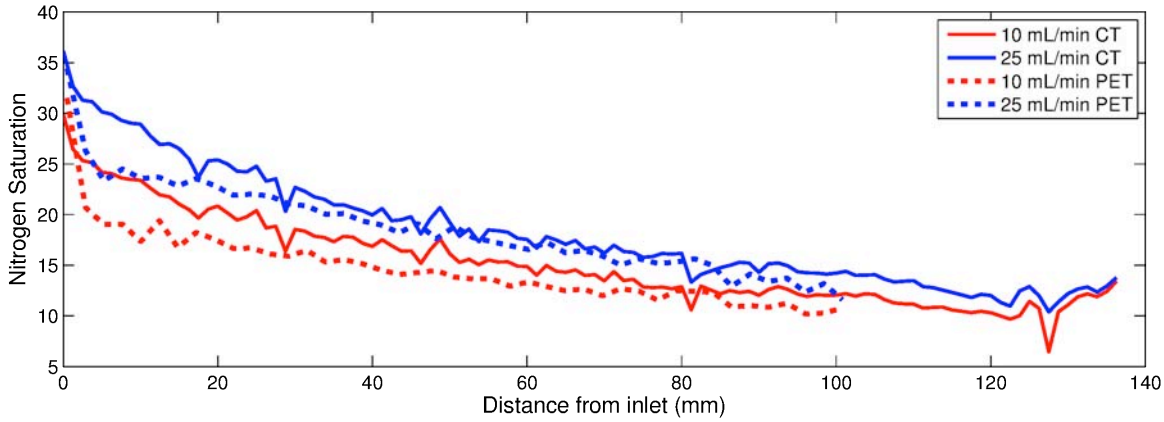

Figure 4: Slice average nitrogen phase saturations along the length of the core for different flow rates. Solid lines are measured during a drainage experiment using CT to calculate saturations, dashed lines are slice average values measured during a separate drainage experiment using micoPET to measure saturations.

Streamtube permeability and porosity calculation

With the measurement of the inlet slice saturation from both the microPET and CT experiments, the core average capillary pressure can be estimated using the method described in [3]. Four different plug samples were also used to measure capillary pressure using the Mercury Injection Capillary Pressure (MICP) technique with a Micromeritics Autopore IV. The results of these four curves were fit with a Brooks-Corey capillary pressure function (Equation 3). The fitting parameters used were λ=1.6, S_{wir} =0.21, and Pc_{entry} = 1.2 psi.

$$Pc(S_w) = Pc_{entry}\left(\frac{S_w - S_{wir}}{1 - S_{wir}}\right)^{-1/\lambda} \qquad (3)$$

Using the fitted capillary pressure function and the phase saturation maps it is possible to describe the permeability of every voxel in the core using a simplified version of the method developed by Krause et al [4] and described in Equation 4 and 5.

$$k_i = \phi_i \frac{1}{\overline{P_c}^2}\left[\sigma_{w/nw}\cos\theta_{w/nw} J(S_{w,i})\right]^2 \qquad (4)$$

Where k_i is the voxel permeability, φ_i is the voxel porosity (measured with CT), Pc bar is the capillary pressure of the slice containing voxel *i*, using the slice average saturation. Sigma and theta are surface tension and contact angle respectively and $J(S_{w,i})$ is the dimensionless J-function described in greater detail in Equation 5.

$$J(S_{w,i}) = \frac{P_c(S_{w,i})}{\sigma_{w/nw}\cos\theta_{w/nw}}\sqrt{\frac{k_c}{\phi_c}} \qquad (5)$$

Where k_c is the core average permeability, φ_c is the core average porosity, and $Pc(S_{w,i})$ is the capillary pressure of the voxel *i*, using the voxel saturation measured during the CT experiment at 10 mL/min.

With the 3D permeability map, the permeability of each voxel along the axis of the core is then harmonically averaged to calculate the permeability of each 1D streamtube. The streamtube permeability and porosity of the core are shown in Figure 5. The porosity and permeability maps highlight heterogeneity in the core in the form of bedding planes which run parallel to the axis of the core. These bedding planes visually have variable grain size and lead to layers with permeability values as high as 40 mD and as low as 17 mD.

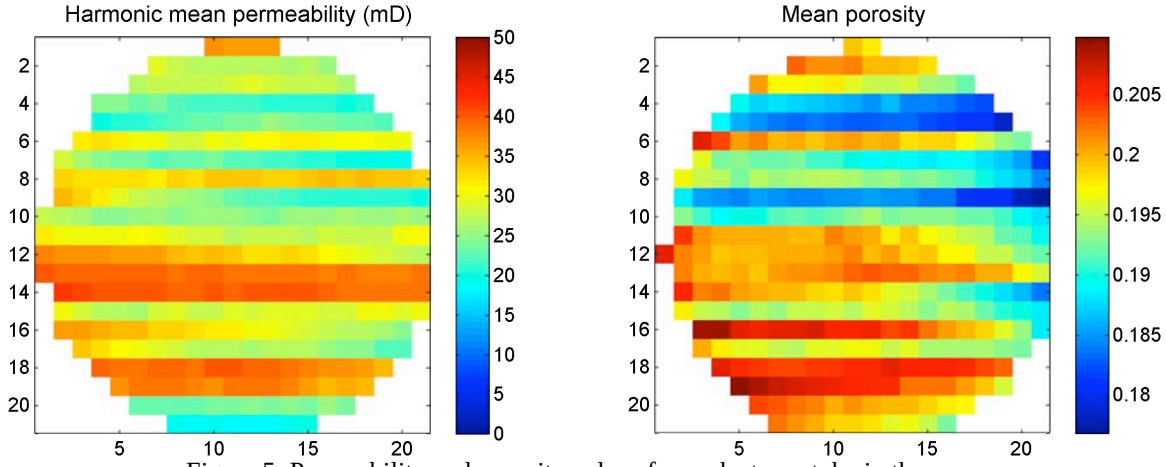

Figure 5: Permeability and porosity values for each streamtube in the core.

PET Tracer Pulse Analysis

One of the greatest strengths of microPET imaging is the ability to quantitatively visualize tracer flow inside the core during single or multiphase experiments. Using the first 30 minutes of the microPET experiment described above, we are able to image the tracer pulse migration and pulse spreading due to diffusion and dispersion as the pulse of tracer travels through the core (colored circles in Figure 7).

Results of the PET pulse experiment can then be fit with the discrete pulse solution to the Advection-Dispersion Equation [12].

$$C(z,t) = \frac{C_0}{2}\left[\left(\operatorname{erfc}\frac{z - v_z t_0}{2\sqrt{D_z t_0}} + \exp\frac{v_z z}{D_z}\operatorname{erfc}\frac{z + v_z t_0}{2\sqrt{D_z t_0}}\right) - \left(\operatorname{erfc}\frac{z - v_z t_s}{2\sqrt{D_z t_s}} + \exp\frac{v_z z}{D_z}\operatorname{erfc}\frac{z + v_z t_s}{2\sqrt{D_z t_s}}\right)\right] \quad (6)$$

Where C_0 is the injected radiotracer concentration, v_z is the average linear velocity along each streamtube, z is the distance from the inlet of the core, t_0 is the start time of tracer injection, t_s is the stop time of tracer injection, and D_z is the longitudinal dispersion coefficient. The longitudinal dispersion is described by $D_z = \alpha\ v_z$, where α is the transverse dispersivity. The ADE is fit to the PET data by determining the dispersivity of the entire core and by determining the dispersivity of the streamtubes. Here we assume the dispersivity in all of the streamtubes is equal however the dispersion coefficients are different due to different linear velocities arising from permeability and porosity heterogeneity. Figure 6 shows the solution for the entire core with a dispersivity of 0.27 cm (dashed lines), and the solution for the streamtube model with a dispersivity of 0.11 cm (solid lines). These results agree well with those of Pini et al [5] showing that the streamtube model yields significantly lower dispersivity than the 1D model. The discrepancy for both the 1D and streamtube model fitting at early time is likely due to tracer mixing in the coreholder inlet dead volume which creates a more disperse tracer injection pulse.

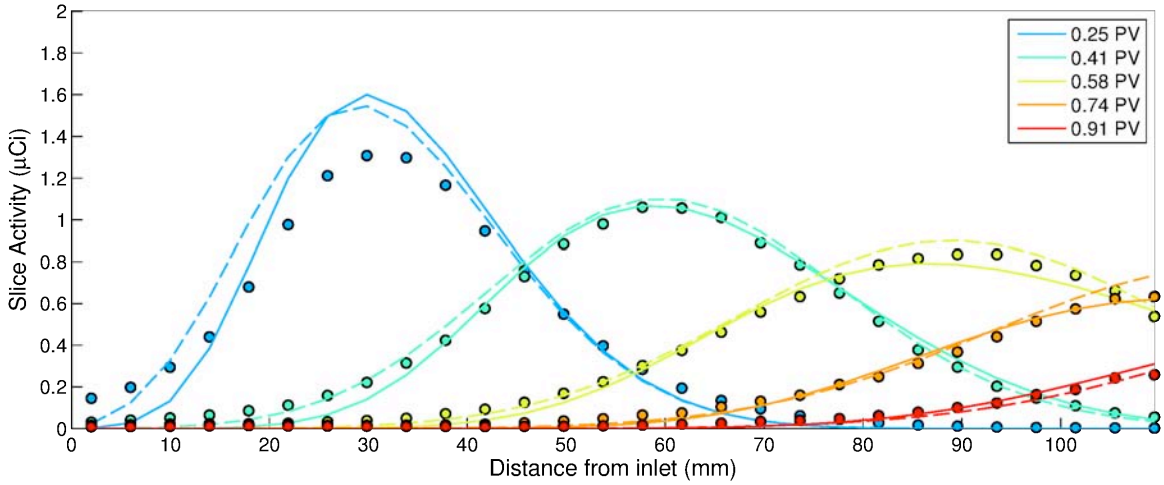

Figure 6: Slice average activity levels along the length of the core at different times during the pulse injection experiment. PET data, 1D ADE solution, and the streamtube ADE solution are indicated by the circles, dashed lines, and solid lines respectively.

The ADE solutions can also be compared at the voxel level with results from the PET tracer data. Figure 7 compares the radiotracer concentration in the slice down the center of the core for the microPET scan, the ADE streamtube solution, and the core-average solution. The voxel-based analysis indicates that the heterogeneity in the core creates significant transverse dispersivity which is not captured in the 1D streamtube analytical approximation. Fully 3D numerical simulation work is ongoing to better validate the sub-core scale porosity, permeability, and dispersivity.

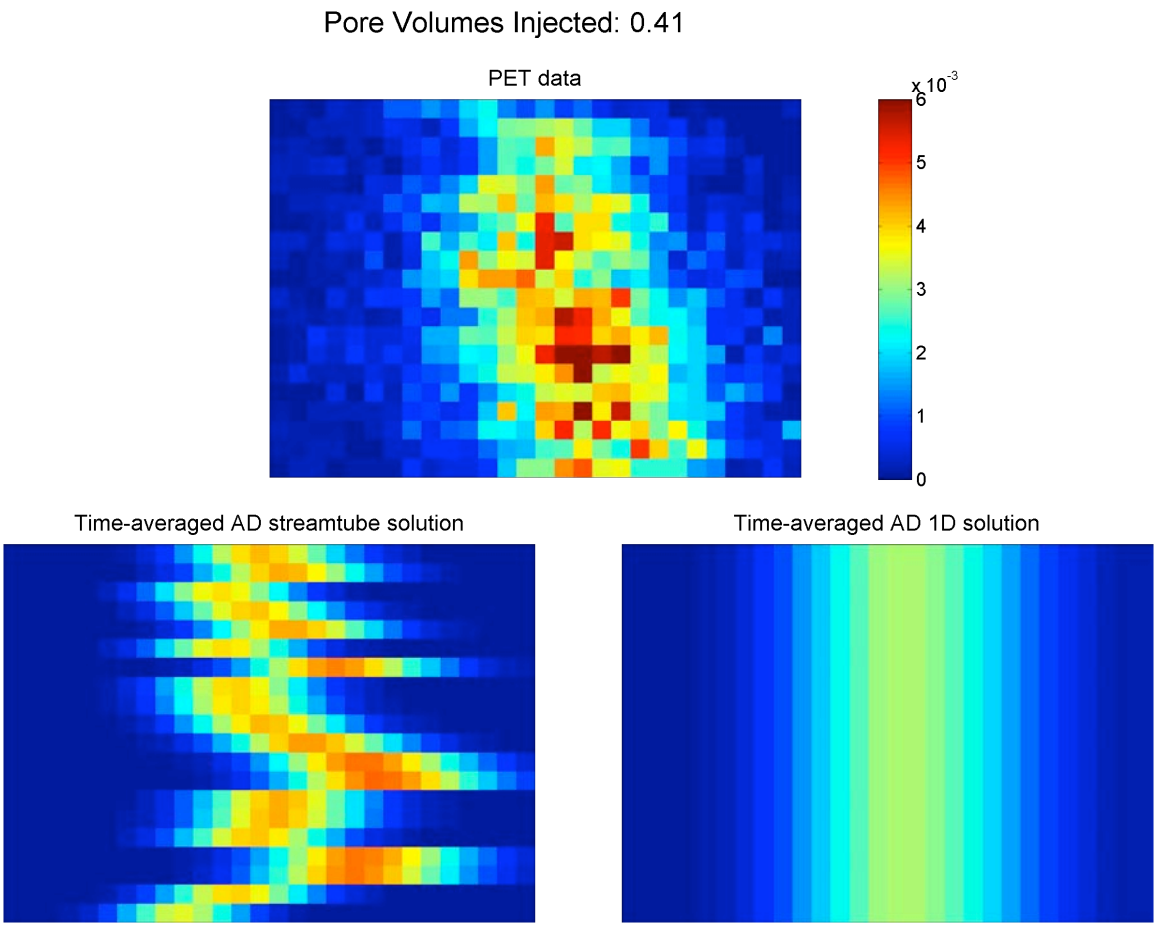

Figure 7: Comparison of PET tracer migration (top), analytical streamtube tracer migration (lower-left), and core-average 1D analytical tracer migration (lower right) after 0.41 PV of water have been injected following tracer injection. The tracer is injected from left to right. The colorbars of all three plots range from 0 to 0.006 μCi.

CONCLUSION AND FUTURE WORK

This study is one of the first instances of using microPET imaging to quantify flow in porous media and is the first study in which phase saturation measurements made using PET have been validated through repeated experiments using the well-established X-ray CT methods for saturation measurement. One of the greatest benefits of using PET imaging is the ability to quantify the flow behavior of tracers that do not measurably change the properties of the tracer fluid. The dynamic imaging and increased signal to noise ratios of microPET allow in-situ tracer visualization, and more importantly quantification, of both single and multiphase flows at the continuum scale. In future studies microPET scans, complemented by CT data, will be used to further validate core wide permeability maps, dispersion and diffusion analysis, and better understand the dynamic and steady state flow behavior during drainage and imbibition experiments.

ACKNOWLEDGEMENTS

This work is funded by the Global Climate Energy Project, the Stanford Center for Carbon Storage, and the Department of Energy Resources Engineering. The Inveon DPET (microPET) scanner was funded by NIH grant number 1S10OD018130-01. Nick Vandehey, James O'Neil, Tim Doyle and Frezghi Habte provided essential radioisotope handling training, PET scanner training, instruction, and advice. Yaxin Li, Yao Yao, Daniel Hatchell, and Cindy Ni provided invaluable assistance in moving laboratory equipment across campus.

REFERENCES

1. Levin, C.S. and Hoffman, E.J., "Calculation of positron range and its effect on the fundamental limit of positron emission tomography system spatial resolution," *Physics in medicine and biology*, (1999) **44,** 3, 781-799.
2. Krause, M. H., Perrin, J. C., & Benson, S. M., "Modeling permeability distributions in a sandstone core for history matching coreflood experiments," *SPE Journal*, (2011) **16**, 04, 768-777.
3. Pini, R., Krevor, S.C.M., Benson, S.M., "Capillary pressure and heterogeneity for the CO2/water system in sandstone rocks at reservoir conditions," *Advances in Water Resources*, (2012) **38**, 48-59.
4. Krause, M., Krevor, S., Benson, S.M., "A Procedure for the Accurate Determination of Sub-Core Scale Permeability Distributions with Error Quantification," *Transport in Porous Media*, (2013) **98**, 565-588.
5. Pini, R., Vandehey, N.T., Druhand, J., O'Neil, J.P., Benson, S.M., "Quantifying solute spreading and mixing in reservoir rocks using 3D PET imaging," *Journal of Fluid Mechanics*, (2016), **796**, 558-587.
6. Loggia, D., Gouze, P., Greswell, R., and Parker, D.J., "Investigation of the geometrical dispersion regime in a single fracture using positron emission projection imaging," *Transport in Porous Media*, (2004) **55**, 1-20.
7. Kulenkamp, J., Grundig, M., Richter, M., and Enzmann, F, "Evaluation of positron-emission-tomography for visualisation of migration processes in geomaterials," *Physics and Chemistry of the Earth*, (2008) **33,** 14-16, 937-942.
8. Ferno, M.A., Gauteplass, J., Hauge, L.P., Abell, G.E., Adamsen, T.C.H., Graue, A., "Combined PET and CT to visualized and quantify fluid flow in sedimentary rocks," *Advances in Water Resources*, (2015) **51**, 7811-7819.
9. Maucec, M., Dusterhoft, R., Rickman, R., Gibson, R., Buffler, A., and Heerden, M.V., "Imaging of Fluid Mobility in Fractured Cores Using Time-lapse Positron Emission Tomography," *SPE 166402*, (2013) 1-12.
10. Hudson, H.M., Larkin, R.S., "Accelerated Image Reconstruction Using Ordered Subsets of Projection Data," *IEEE Transactions on Medical Imaging*, (1994) **13**,4, 601-609.
11. Akin, S. Kovscek, A.R., "Computed tomography in petroleum engineering research," *Geological Society, London, Special Publications*, (2003) **215**, 25-38.
12. Bedient, P.B., Rifai, H.S., Newell, C.J., "Ground Water Contamination: Transport and Remediation, 2nd Edition," *Prentice Hall*, (1999)